coatings

MDPI

Article

Deposition and Characterisation of a Diamond/Ti/Diamond Multilayer Structure

Awadesh Kumar Mallik [1,2,3,*], Fernando Lloret [4], Marina Gutierrez [5], Rozita Rouzbahani [1,2], Paulius Pobedinskas [1,2], Wen-Ching Shih [1,6] and Ken Haenen [1,2]

1 Institute for Materials Research (IMO), Hasselt University, 3590 Diepenbeek, Belgium; rozita.rouzbahani@uhasselt.be (R.R.); paulius.pobedinskas@uhasselt.be (P.P.); wcshih@ttu.edu.tw (W.-C.S.); ken.haenen@uhasselt.be (K.H.)
2 IMOMEC, IMEC VZW, 3590 Diepenbeek, Belgium
3 Temasek Laboratories, Nanyang Technological University, Singapore 637553, Singapore
4 Department of Applied Physics, University of Cádiz, 11510 Puerto Real, Spain; fernando.lloret@uca.es
5 Department of Materials Science and Metallurgical Engineering, University of Cadiz, 11510 Puerto Real, Spain; marina.gutierrez@uca.es
6 Department of Electrical Engineering, Tatung University, Taipei 10451, Taiwan
* Correspondence: awadesh.mallik@gmail.com or awadesh.mallik@ntu.edu.sg

Abstract: In this work, a diamond/Ti/diamond multilayer structure has been fabricated by successively following thin-film CVD and PVD routes. It has been found that a combined pre-treatment of the silicon base substrate, via argon plasma etching for creating surface roughness and, thereafter, detonation nanodiamond (DND) seeding, helps in the nucleation and growth of well-adherent CVD diamond films with a well-defined Raman signal at 1332 cm^{-1}, showing the crystalline nature of the film. Ti sputtering on such a CVD-grown diamond surface leads to an imprinted bead-like microstructure of the titanium film, generated from the underlying diamond layer. The cross-sectional thickness of the titanium layer can be found to vary by as much as 0.5 µm across the length of the surface, which was caused by a subsequent hydrogen plasma etching process step of the composite film conducted after Ti sputtering. The hydrogen plasma etching of the Ti–diamond composite film was found to be essential for smoothening the uneven as-grown texture of the films, which was developed due to the unequal growth of the microcrystalline diamond columns. Such hydrogen plasma surface treatment helped further the nucleation and growth of a nanocrystalline diamond film as the top layer, which was deposited following a similar CVD route to that used in depositing the bottom diamond layer, albeit with different process parameters. For the latter, a hydrogen gas diluted with PH_3 precursor recipe produced smaller nanocrystalline diamond crystals for the top layer. The titanium layer in between the two diamond layers possesses a very-fine-grained microstructure. Transmission electron microscopy (TEM) results show evidence of intermixing between the titanium and diamond layers at their respective interfaces. The thin films in the composite multilayer follow the contour of the plasma-etched silicon substrate and are thus useful in producing continuous protective coatings on 3D objects—a requirement for many engineering applications.

Keywords: diamond; titanium; composite; chemical vapour deposition (CVD); physical vapour deposition (PVD)

Citation: Mallik, A.K.; Lloret, F.; Gutierrez, M.; Rouzbahani, R.; Pobedinskas, P.; Shih, W.-C.; Haenen, K. Deposition and Characterisation of a Diamond/Ti/Diamond Multilayer Structure. *Coatings* **2023**, *13*, 1914. https://doi.org/10.3390/coatings13111914

Academic Editor: Mikhaïl Rodionovich Baklanov

Received: 20 September 2023
Revised: 3 November 2023
Accepted: 7 November 2023
Published: 8 November 2023

1. Introduction

Diamond and titanium are both important engineering materials. There are mechanical, thermal, electrical, and biomedical applications, where the titanium metal and the diamond ceramic can be used together [1–3]. Titanium and its alloys [4] are widely used as medical implant materials due to their excellent ductility, but they have poor tribological properties [5], which can be overcome by making a composite with wear-resistant diamond ceramics [6–8]. Both of them are chemically inert and biocompatible with many biological

applications [9–13]. Researchers (including from Hasselt University) have deposited diamond coatings on Ti substrates [14–18], sometimes using intermediate layers [19,20] such as SiC [21–23] via a CVD deposition route. Hydrogen diffusion into the Ti structure leading to microstructure coarsening has been reported to be a CVD synthesis issue [24]. Due to the various applications that diamond–Ti composite material may find in electrode [25], thermal [26], mechanical [27], and biological fields, it is important to study this combination of materials.

Joining diamond films with other metals [28] is an important post-CVD processing step for integrating different components into making a device. Researchers have successfully brazed diamond coatings on Ti alloy substrates using Ti-Cu-Ag or Cu-Sn-Ti fillers and studied their interfacial microstructures [29,30]. On the other hand, Ti films have been deposited via sputtering for many engineering applications [31–36]. Some researchers have also coated diamond powders with Ti via magnetron sputtering to improve their oxidation and graphitization resistance [37]. There are also papers on magnetron sputtering of Ti and diamond-like carbon composite films [38], and those dealing with Ti-doped CVD diamond films using Tetra n-butyl titanate as a dopant precursor [39]. The objective of introducing Ti inside the diamond crystal structure was to reduce the stress by improving bonding with the base material by creating a strong interface [40]. Due to the reaction between Ti and diamond, it can potentially act as bonding material [41]. Here, one Ti layer is deposited between two diamond layers to study how well they adhere to each other. Researchers have earlier investigated the brazing interfaces of diamond with other metals using titanium-based filler materials. The present work will also throw light upon the interfacial structure of the novel diamond/Ti/diamond composite. As the CVD of diamond on the Ti substrates reportedly leads to adhesion problems [42], we have additionally enhanced the diamond nucleation on the silicon substrate by combining substrate roughening and the detonation nanodiamond (DND)-seeding technique for promoting substrate adhesion. Moreover, hydrogen gas in the CVD recipe was reported to influence the Ti film microstructure [36]. Therefore, an additional hydrogen plasma CVD treatment was also conducted on the Ti–diamond composite film before the deposition of the top CVD diamond layer, which was grown without additional seeding steps. To avoid microstructure coarsening [36], diluted phosphine in hydrogen gas was used in the precursor recipe for growing the top diamond layer. The incorporated phosphorus atom reportedly produces a finer nanocrystalline diamond microstructure [43,44]. This synthesises a smoother top layer of the composite film.

As discussed above, the other researchers find investigating Ti–diamond composite structures for various applications such as electrodes, thermal management, mechanical, etc., to be important. Moreover, multi-layer processing is studied here because the importance of joining diamonds with metals and the role of Ti in interfacial bond formation has reportedly been significant. The motivation of the research is to understand the interaction of diamond with Ti as a composite layered structure by investigating their adhesion, their reaction under hydrogen plasma, the effect of substrate roughness, and its influence on the layered microstructure and other CVD and PVD growth characteristics, which has not been studied before.

2. Materials and Methods

2.1. Ar^+ Ion Milling of the Base Substrate

A set of silicon substrates (p-type, (100) orientation) was treated with Ar^+ plasma inside a PVD sputtering chamber [45]. The substrates were kept at a bias voltage power of 150 W, and the Ar gas was flown at 100 sccm. Plasma treatment was conducted for a total of 100 min in periods of 20 min each to avoid excessive heating of the reactor component, with four intermittent periods of cooling. A second set of samples underwent O_2 plasma cleaning to remove the organic substances that are always present on their as-received surfaces. Such O_2 plasma treatment was conducted for 10 min with 35 sccm flow rates of gas at 50 W bias power.

2.2. DND Seeding of the Base Substrates

Both sets of Ar- and O_2-treated silicon substrates were seeded with detonation nanodiamond particles to enhance the nucleation and growth of diamond crystals during CVD processing. DND powders were mixed in de-ionised water by 0.05 wt% and sonicated to produce a water based DND suspension. A single drop of the suspension was added onto the Si surface, which was vacuum mounted onto a spin coater. A monolayer coating of the DND seeds was obtained [46] after spinning for 40 s at a speed of 4000 rpm, with short rinsing with de-ionised water and successive drying by a nitrogen gun.

2.3. CVD of Microcrystalline Diamond (MCD)—Bottom Layer

An innovative linear antenna microwave plasma-enhanced CVD (LAMWCVD) reactor (also referred elsewhere as surface wave plasma-enhanced CVD apparatus) was used to grow diamond. In contrast to resonant cavity CVD reactors, where the typical diamond growth temperature window is 700–1100 °C at sub-atmospheric pressures of 10–100 Torr, inside the surface wave plasma CVD reactor, there is travelling microwave along the length of the antenna which enables the production of diamond films at low temperatures of 300–400 °C and very low pressures of 0.2–1 Torr. However, this low-temperature/low-pressure process grows diamond films at slow growth rates of 5–20 nm per hour [47]. Therefore, it takes several hours of deposition to grow continuous thick diamond films. The DND-seeded substrates were first loaded onto the molybdenum stage of the CVD reactor, and the distance of the quartz tube to the stage was adjusted to 5 cm height before evacuating the chamber to a base pressure of 6×10^{-4} Torr. After reaching the desired base pressure, the precursor gases H_2, CH_4, and CO_2 were flown into the chamber at 133.5 sccm, 7.5 sccm, and 9 sccm rates, respectively. The addition of CO_2 in the precursor recipe helps to remove graphitic carbon (as it contains oxygen) and promote the growth of better-quality diamond films. The working pressure, with 150 sccm total volumetric flow rate, was recorded to be 0.23 mTorr. Thereafter, two 2.45 GHz magnetrons were switched on gradually to a total average output power of 2800 W in continuous wave mode. Since there was no extra heater, it took more than 60 min to achieve a stable substrate temperature of 400 °C, solely heated by the microwave plasma. The substrate temperature was measured via a thermocouple placed underneath the substrate stage (therefore protected from the plasma environment).

2.4. PVD Sputtering of Ti Interlayer

After characterising the diamond-coated silicon substrates via different techniques (as described in Section 2.7), a Ti film was sputtered on top of the diamond layer. A commercially available 4-inch Ti-target was used for sputtering with 100 sccm flow rates of Ar plasma in a line-of-sight biasing arrangement PVD chamber. The throttle valve was kept open at 50% to maintain a working pressure of 10^{-2} Torr, while the starting base pressure was 10^{-7} Torr. The applied power was 150 W, and the sputtering was conducted, varying from 1 to 10 min, to deposit Ti film of different thickness. The typical sputtered Ti deposition rate was 10 nm per minute.

2.5. Hydrogen Plasma Etching of Ti–Diamond Composite Double Layer

After sputtering, the as-deposited rough surface of the two-layer (Ti + diamond) composite film was etched (smoothened) by hydrogen plasma for 20 min at 40 Torr pressure inside a microwave plasma-enhanced resonant cavity CVD chamber. The applied power was 3000 W with 400 sccm of H_2 gas flow rate. The substrate temperature was recorded around 680 °C via a double-wavelength optical pyrometer (Williamson, model No. PRO 92-400C, Concord, MA, USA). The samples were directly loaded into the CVD chamber from the PVD sputtering chamber.

2.6. LAMWCVD of Nanocrystalline Diamond (NCD) Top Layer

Finally, a second diamond layer was grown on the top of the samples. There was no DND seeding step prior to the growth of the top diamond layer. The CVD diamond growth parameters were like the conditions used earlier for growing the bottom MCD layer, described in Section 2.3. There were only two changes made: (1) the hydrogen precursor gas was diluted with 0.1% PH_3, as phosphorus addition reportedly promotes growth of diamond nanocrystals [43,48]; (2) a substrate heater underneath the molybdenum stage was used to preheat the substrate to 700 °C before starting the LAMWCVD plasma recipe to assist phosphorous incorporation into the diamond crystal lattice.

2.7. Physical Characterisations

Atomic force microscopy (AFM—Bruker MultiMode 8 (Billerica, MA, USA)) was performed in tapping mode to observe the effect of plasma etching and DND seeding efficiency on silicon substrates. The surface roughness was also measured via the stylus profilometer Bruker Dektak XT. The contact angles of the water droplets onto the substrate surfaces were determined via the dataphysics OCA, SCA20 software package. Scanning electron microscopy (SEM–FEI Quanta 200 FEG (Hillsboro, OR, USA)) revealed the as-grown morphology and the cross-sectional film thickness of the multilayers, along with the elemental analysis from energy dispersive X-ray spectroscopy (EDS). Raman spectra were recorded with a HORIBA Jobin Yvon T64000 spectrometer (Irvine, CA, USA) using laser light of 488 nm wavelength at 100× objective length with 30 s of data acquisition time for 5 repetitions. A transmission electron microscope (TEM) Jeol 2100 (Tokyo, Japan) with accelerating voltage of 200 keV in diffraction-contrast mode was used to investigate the diamond/Ti/diamond multilayer structures. TEM samples were prepared via mechanical thinning and ion milling (PIPS from Gatan, Pleasanton, CA, USA).

3. Results and Discussion

3.1. Base Substrate: Argon Plasma Etching and DND Seeding

Figure 1a shows a 10 μm × 10 μm area AFM scan of the Ar^+ ion plasma-treated silicon substrate surface. It has a roughness depth scale from −120 nm to +200 nm. The brighter white spots are as wide as 250 nm, whereas the darker pits are created by heavy ion bombardments during plasma treatment. Figure 1b is the Ar^+ plasma-etched silicon surface after DND seeding. It is not possible to distinguish the individual DND seeds from the pits and valleys that are created by the plasma. However, it is evident from the 3D AFM scan in Figure 1b that the silicon surface does not remain smooth after the plasma treatment by heavy Ar^+ ions, as it is for the DND-seeded untreated silicon substrate surface in Figure 1c,d. Such evidence of substrate surface roughening by argon plasma is further confirmed via a stylus profilometer scan. The roughness was about R_a = 11 nm, measured with the stylus profilometer (scan length 4 mm) for the Ar^+ plasma-treated silicon surface, whereas the roughness for the as-received (after O_2 plasma cleaning) silicon surface was approximately 1 nm. The hydrophilicity of the substrate surfaces, as measured via the water droplet contact angles, was enhanced with Ar^+ plasma etching in comparison to the oxygen plasma cleaning of Si. The contact angle becomes 0° after Ar^+ bombardment, while a value of 36° is found for the oxygen plasma-treated silicon surface. There were many more surface irregularities (Figure 1a, $2.6 \times 10^{13}/cm^2$) on the Ar^+ plasma-treated surface, which helps in holding the greater number of DND seeds necessary for CVD growth of diamond films. It is indeed evident that the surface irregularities, and therefore the trapped DND seeds inside of the individual grooves, are considerably higher in Figure 1b as compared to 1c or 1d. Moreover, the mechanical polishing marks visible on the as-received wafer (Figure 1d,f) also disappeared after Ar^+ plasma treatment (Figure 1b). Figure 1e,c shows the corresponding 2D images of Figure 1b,d over equivalent scan areas. The nucleation density calculated on the DND-seeded as-received O_2 plasma-cleaned substrate (1 μm × 1 μm area AFM scan) was $2 \times 10^{10}/cm^2$. However, it was difficult to distinguish the DND seeds from the surface irregularities present in the 5 μm × 5 μm area AFM scan in Figure 1b. However,

the DND seed population or the surface roughness, necessary for diamond nucleation and growth during CVD, is certainly enhanced for the Ar^+ plasma-etched base substrate. Rabinovich et al. [49] previously showed that the nanoscale surface roughness plays an important role in determining the adhesion force between the interacting particles and surfaces. The adhesion force starts decreasing for low surface roughness (≈1 nm); however, the same adhesion force increases again when the roughness becomes more than 10 nm. The Ar^+ plasma-treated surface had higher roughness (11 nm) than the as-received Si surface (O_2 cleaned ≈ 1 nm), which helped in enhancing the DND seeding efficiency.

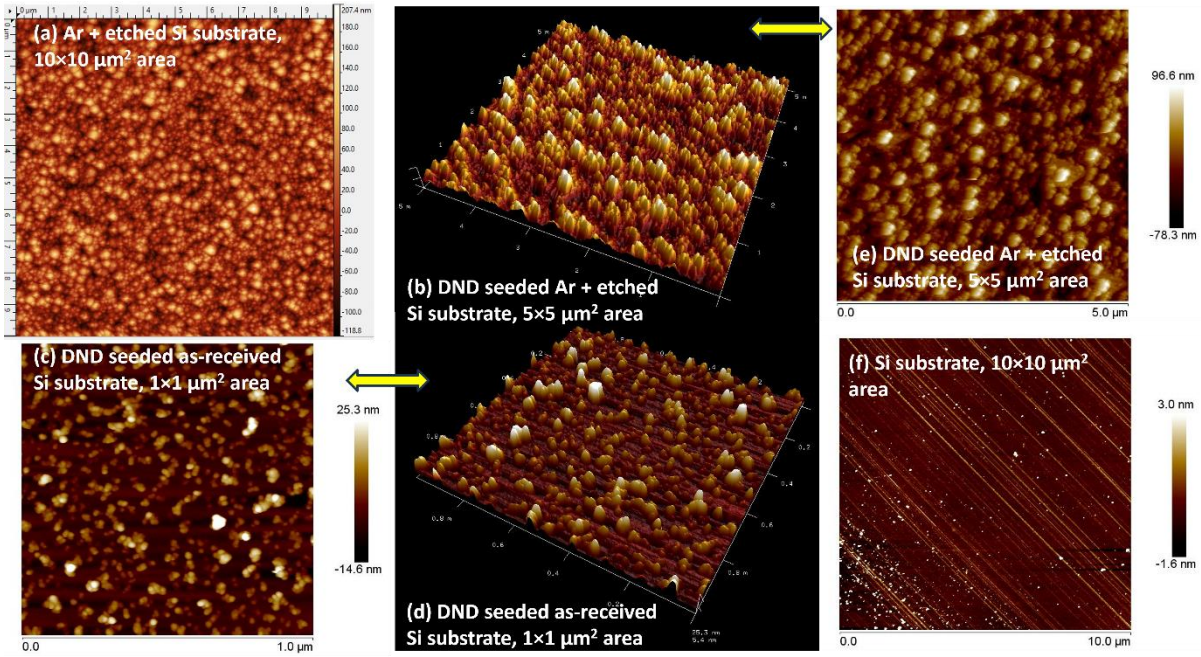

Figure 1. Base substrate AFM images of (**a**) Ar^+ plasma-etched, 2D; (**b**) DND-seeded, Ar^+ plasma-etched, 3D; (**c**) DND seeded, as-received (O_2 plasma-cleaned); 2D, (**d**) DND-seeded, as-received (O_2 plasma cleaned), 3D; (**e**) DND-seeded, Ar^+ plasma-etched, 2D; and (**f**) Si substrate, 2D.

3.2. First Layer of MCD Grown by LAMWCVD

Figure 2 shows SEM micrographs of the diamond coating grown by LAMWCVD over a 3-day long deposition period on an Ar^+ plasma-treated silicon substrate. It is found that the diamond coating has a bi-modal grain size distribution. The background microstructure is a NCD matrix in which there are uniformly scattered MCD grains. The shape of the MCD grains appear to be square in shape from Figure 2a, but at the higher magnification of 15 kX, diamond octahedrals become visible. At a yet higher magnification of 60 kX, the apparent square-shaped MCD grains are found to be the top surfaces of the grown cubo-octahedral diamond crystals. However, the sample was charging under the SEM beam, which may be due to the tip-like features of the cubo-octahedrals of the diamond grains. The square/cubo-octahedrals are not single grains but are composed of individual NCDs. Further investigation is necessary in order to understand the exact growth features of diamond grains. The diagonal length of one such cubo-octahedral is found to be 1.3 µm, as shown in Figure 2c.

3.2.1. LAMWCVD Growth Rate

Figure 3a shows the cross-sectional view of the diamond coating grown over the base substrate over a 3-day long LAMWCVD deposition run period. The MCD thickness was found to be about 2.5 µm. As expected, due to the low-temperature and low-pressure environment inside the surface wave plasma-enhanced CVD reactor, the diamond grows in vertical columns at a very slow growth rate of 39 nm/hr. The interesting point to be noticed

is that the length of the CVD-grown diamond columns are not very different in size from the lateral size of the MCD grains found on the top surface SEM image in Figure 2. The diamond crystals grown inside a resonant cavity CVD reactor generally have a very high aspect ratio, with long columns. This is found not to be the case for the diamond crystals growing inside surface wave plasma CVD reactor [47]. However, the uneven length of the MCD columns (Figure 3a) along the z-direction produced an uneven rough top surface morphology, with MCD grains scattered in an NCD matrix (Figure 2). Such roughness is not desired for many industrial engineering applications. Therefore, it was then necessary either to plasma-polish (Section 2.5) the as-grown MCD films or to use a different CVD recipe for subsequently growing a smoother NCD film (as described in Section 2.6).

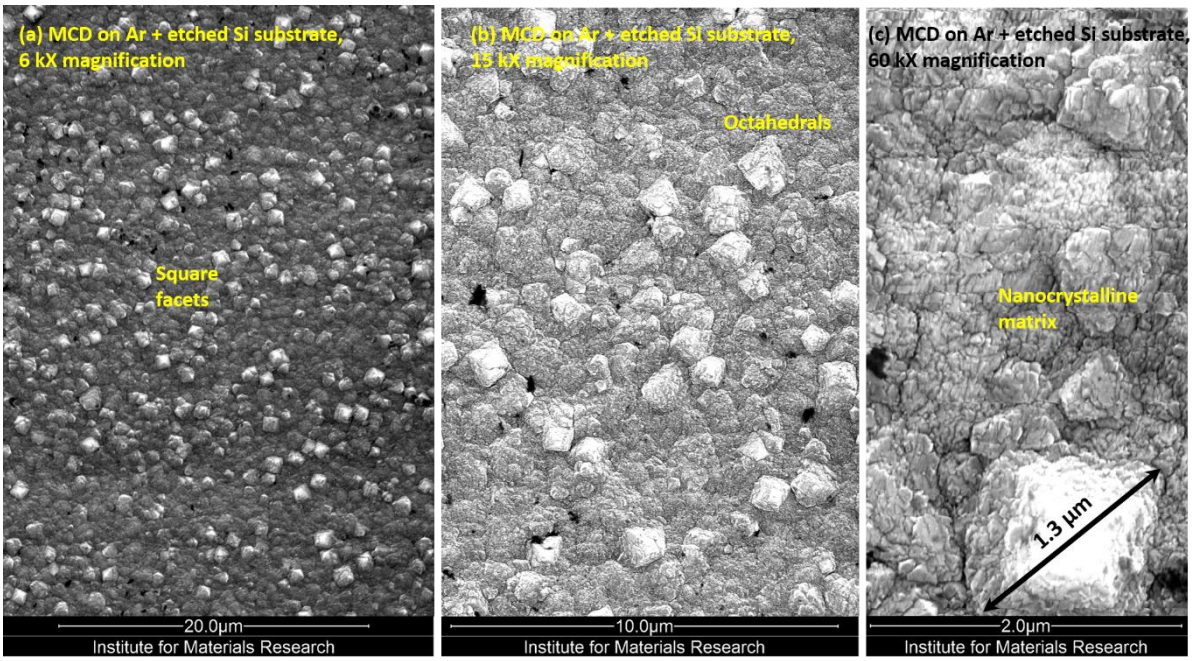

Figure 2. SEM micrographs of the LAMWCVD grown bottom layer of the MCD and NCD bi-modal morphologies at (**a**) 6 kX, (**b**) 15 kX, and (**c**) 60 kX magnifications.

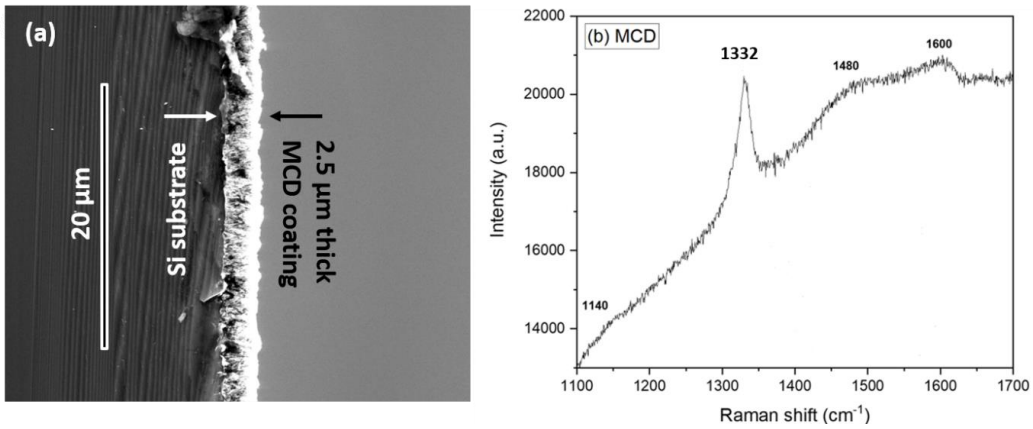

Figure 3. (**a**) Cross-sectional SEM image of the MCD columnar growth. (**b**) Raman spectra of the MCD.

3.2.2. Diamond Raman Signal

The Raman spectrum from a diamond film [50,51] grown on an Ar^+ plasma-etched Si, deposited during a 3-day long LAMWCVD run, is shown in Figure 3b. The sp3-bonded carbon peak appears at 1332 cm^{-1}. The FWHM of this peak is found to be around

20 cm^{-1}. There are also small bumps around 1140 cm^{-1} and 1480 cm^{-1}, which correspond to nanocrystalline diamond (ν_1) and trans-polyacetylene (TPA) phases deposited along with the pure diamond sp3 phase. The crystalline graphite G peak is also found to be present at 1600 cm^{-1}; however, the disordered graphite D peak is not found to be prevalent in the Raman spectrum.

3.3. Ti PVD Sputtering and H_2 Plasma-Etching of Ti-MCD Composite Layer

After the LAMWCVD growth of the diamond, a Ti film was sputtered onto the MCD microstructure distributed in the NCD matrix. The top surface microstructure (Figure 4a) is also nanocrystalline in nature, with rounded micron sized granular features present throughout the matrix. There are cracks present in the microstructure, as also found previously by researchers with respect to a sputtered Cr layer [52]. Some of the grains are loosely bound to the bottom layer. The as-grown diamond surface had a certain roughness. A thin layer of sputtered Ti followed the contour of the rough, as-grown diamond surface. Due to the large difference in thermal expansion coefficients between Ti and diamond, the surface crack appeared unavoidably. The cross-sectional SEM image (Figure 4b) shows the Ti PVD-sputtered film grown over LAMWCVD diamond layer on the Ar^+ plasma-treated silicon substrates. It is to be noticed that the argon plasma-treated substrate has deep grooves and pits (Figure 1a,b), which helped the diamond film to anchor firmly into the silicon, enabling better film adhesion. The thickness of the CVD-grown diamond columns vary in length from point to point. Figure 4b shows a uniform thickness of 2.45 μm, whereas it was different in Figure 3a before Ti sputtering. The sputtered Ti film was also found to vary in thickness from point to point by as much as 0.5 μm in depth. Figure 3a also shows variation in the diamond film thickness from point to point across the surface length, with respective differences of as much as 0.5 μm. However, the wide variation in Ti film thickness found in Figure 4b was not due to the variation in lengths of the CVD-grown diamond columns; it was due to the hydrogen plasma treatment of the Ti–diamond composite films (Section 2.5). There was very little time interval given in between Ti sputtering and the subsequent H_2 plasma treatment. The sample was loaded into the CVD reactor as soon as it was sputter-coated to avoid unwanted atmospheric oxidation of the freshly coated Ti surface. Hydrogen plasma etched the Ti film to even expose the underlying diamond layer in some places, as it is found in Figure 5a. The underlying diamond film was also etched, becoming very even and smooth. There were no bimodal MCD and NCD features visible (Figure 5a) as it was earlier found in Figure 2. It could be imagined that the titanium film followed the contour of the MCD-filled NCD matrix in Figure 2, which was apparent even after the hydrogen plasma treatment of the Ti–diamond composite film. There were bead-like granular features, which must have been imprinted onto the top Ti film from the underlying diamond microstructure. The top titanium film also shows signs of delamination from the diamond surface. The electron diffraction elemental analysis of the EDS spectra in Figure 5b shows a very small amount of Ti, even smaller than Si, which might have originated from the underlying substrate and might be a contamination from the CVD reactor used for hydrogen plasma etching [47]. The as-grown film surface unevenness was greatly reduced by the hydrogen CVD plasma etching. No DND-seeding step was further required before the subsequent growth of diamond layer on top of the hydrogen plasma-etched Ti film. Figure 5a shows that there are exposed bottom layer diamond surfaces from place to place, which helped in the nucleation and growth of the next diamond layer. Researchers have previously reported a similar seeding method via a carbon transport phenomenon from the buried layers [52–54].

It is to be noted that Figures 4a and 5a are from different regions of the same surface after hydrogen plasma treatment of the Ti sputtered layer. It shows the etching by hydrogen plasma of the surface, surface cracks, and imprinted morphology. Cracks appeared due to the thermal cycles the coating underwent due to sputtering and subsequent hydrogen plasma exposure. However, the surface cracks have not penetrated inside the deposited layers, as evidenced by the cross-sectional SEM image (Figure 4b). Hydrogen plasma

etched out any oxide layer that might have appeared in between samples transferring between two reactors. EDS data (Figure 5b) do not show the presence of any elemental oxygen in the deposited composite layers. The top surface morphology varies from point to point; moreover, the cross-sectional features show height undulations. However, the layers are continuous, perhaps with local phase and height variations (metallic Ti and its carbide). Such local variation (thickness and phases) across the length of the multilayer is also noticed later in the TEM study.

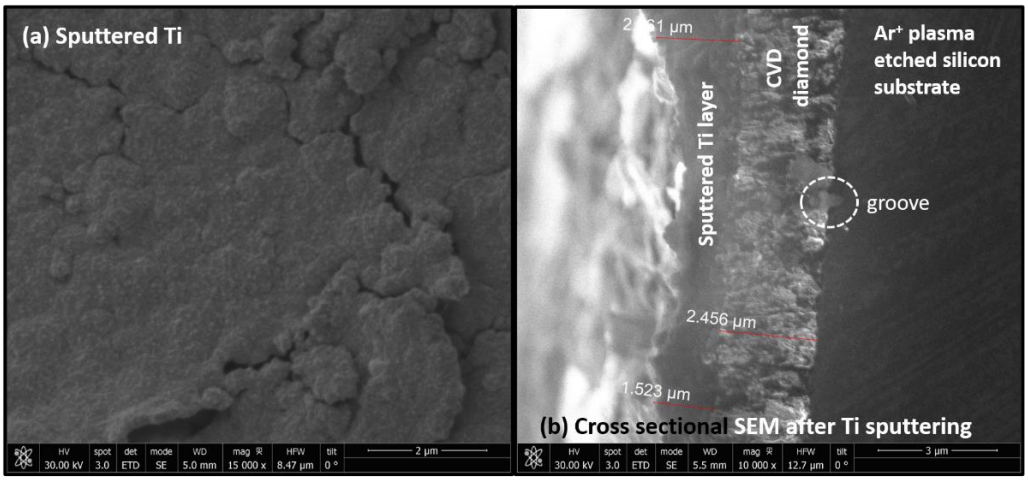

Figure 4. SEM (**a**) surface morphology and (**b**) cross-section of the composite Ti-MCD sample.

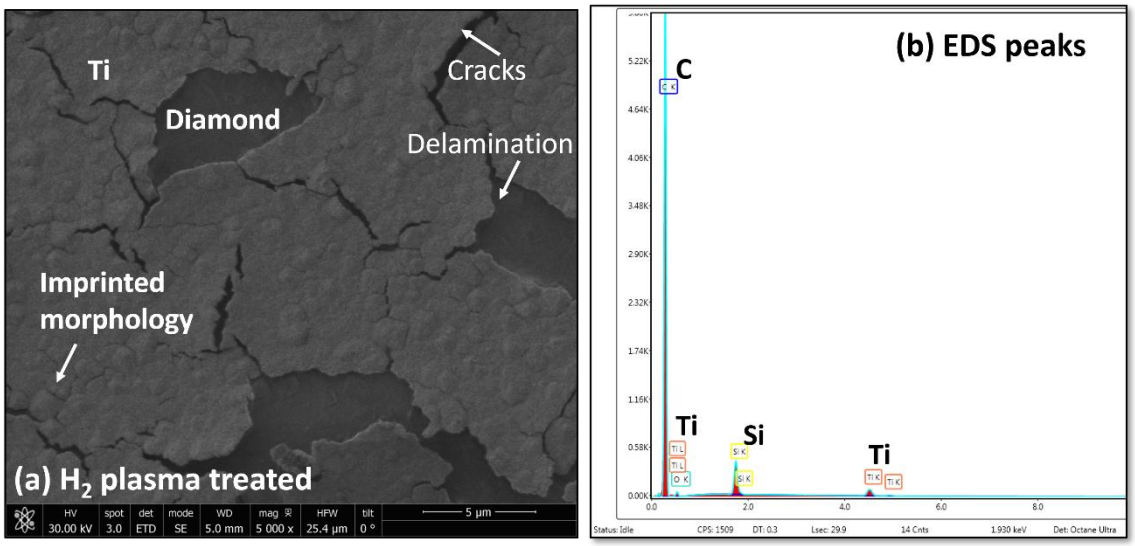

Figure 5. (**a**) SEM image showing hydrogen plasma etching of the Ti-sputtered layer and (**b**) EDS of the image in subfigure (**a**).

3.4. Top Layer NCD Grown by LAMWCVD

Figure 6 shows the CVD-grown diamond morphology of the top layer, deposited inside the same surface wave microwave plasma reactor used earlier to grow microcrystalline morphologies. The deposited morphology is completely different from the earlier CVD-grown diamond film microstructure (Figure 2) grown by the same reactor but without the addition of phosphine and additional substrate heating. In Figure 6, the microstructure of the diamond film looks cigar-like, elongated, and randomly oriented at a lower magnification of 20 kX due to phosphine gas addition in the precursor recipe [43]. At still-higher magnification (Figure 6b), it is found to have an aspect ratio of about 3:1, where the length is 150–200 nm and width of the feature is 70–80 nm. Figure 6c shows that the

individual cigar-like structure is spindle-like in shape, with a broad middle portion and tapered ends. Each elongated structure is again found to be sub-divided into individual diamond nanoparticles of 30–40 nm in size. Earlier research results with nitrogen-doped diamond film showed high-aspect-ratio needle-like microstructures [55]. Therefore, the research question is raised here, i.e., whether P being another Group V element, such as nitrogen, also promotes a high-aspect-ratio diamond grain microstructure in the deposited film. The phosphine-based gas LAMWCVD recipe at an elevated temperature produced unique cigar-like NCD morphology, unlike the MCD-distributed NCD found on the bottom layer of the diamond (produced over long hours of LAMWCVD run). Therefore, the top-layer diamond surface is smoother than the bottom layer as-grown diamond surface.

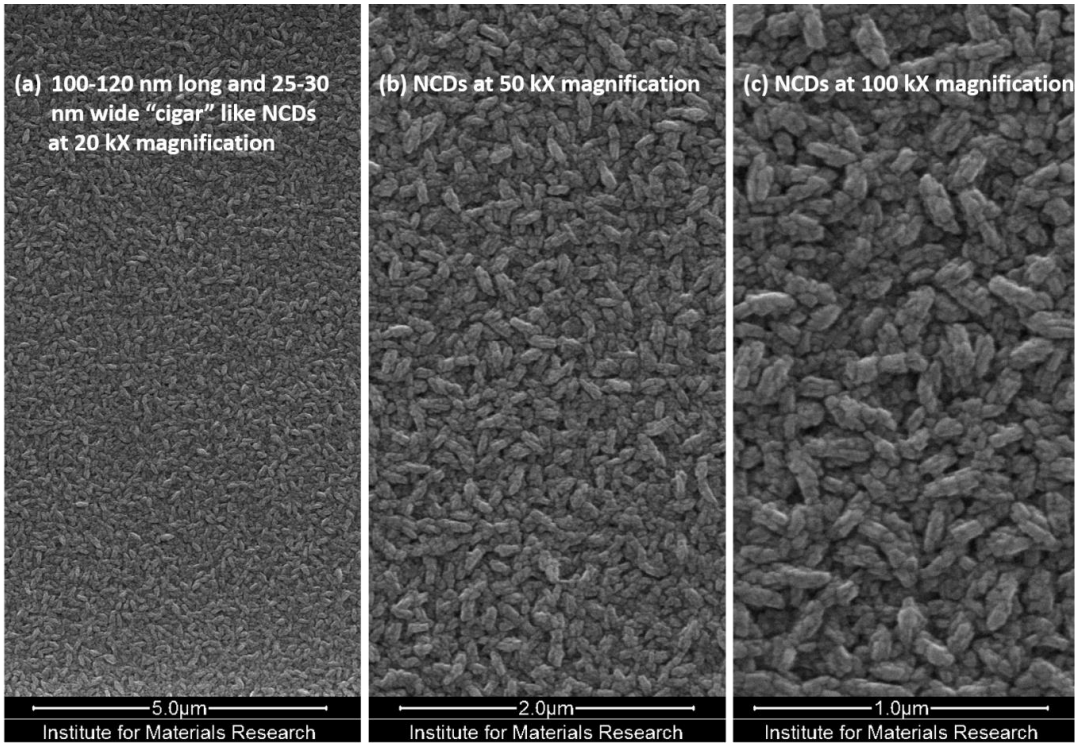

Figure 6. SEM morphologies of the NCDs grown at 700 °C with, 133.5 sccm H_2 (diluted with 0.01% PH_3), 7.5 sccm CH_4, and 9 sccm CO_2 precursor LAMWCVD recipe at (**a**) 20 kX, (**b**) 50 kX, and (**c**) 100 kX magnifications.

Diamond/Ti/Diamond Sandwich Structure: TEM Cross-Section

The NCD layer grown with diluted phosphine at elevated temperature onto the Ti–diamond composite film was further investigated under TEM. A Ti film was found as expected: to be sandwiched in between two diamond layers (Figure 7c). The bottom diamond layer (Figure 7b) prepared using the regular LAMWCVD recipe was found to be more crystalline than the top LAMWCVD-grown diamond layer (Figure 7c) grown with the diluted phosphine recipe. The bottom silicon substrate pre-treated with Ar^+ ion plasma is observed to have many asperities and valleys, which indeed helped to firmly anchor the CVD-grown film layer onto the base substrate, promoting diamond film adhesion. The corresponding crystals have elongated columnar grains starting from the base silicon substrate. There is evidence of a typical literature-reported [27] needle-like structure of TiC penetration into the bottom diamond layer (Figure 7b). Figure 7a also shows that both the top and the bottom interface-layers of the Ti with the adjacent diamond layers are intermixed with each other. Figure 7 shows that the typical thickness of the diamond layers is approximately 250 nm, whereas the Ti sputtered layer has approximately 50 nm thickness. They tally with the deposition time and growth rates of the corresponding LAMWCVD and sputtering processes. It is also known from the literature [27] that Ti has a

propensity to form a dendritic carbide phase in chemical reaction with diamond. Figure 7c shows that although the NCD grains are elongated in the top layer, they are not as big as the bottom-layer diamond columns. Moreover, the intermediate titanium grains are found to be very small and circular in shape (Figure 7c). The substrate surface irregularities created by the argon plasma pre-treatment greatly influenced the growth of the successive diamond and Ti layers. It is found that the crevices found in the AFM (Figure 1a,b) are as deep as 100 nm, as also evidenced by the respective TEM images. Such a substrate surface roughness promoted the growth of CVD diamond elongated grains. The immediate diamond grains, next to the substrate, are nanocrystalline, which is typical when diamond nanoparticles are used as seeds before the diamond layer coalesces, followed by further growth in the z-direction. The base substrate surface seems to have a profound influence on the surface topography of the growing films in the successive layers. Figure 7a shows that each layer follows the contour of the base substrate. Each layer is very uneven in nature, and the final top NCD surface has an undulating wavy feature in tandem with the underlying layers. Figure 7d shows a triangular pyramidal base substrate surface with a hillock structure caused by the Ar^+ plasma etching. Similar triangular features are present all throughout the bottom layer of the diamond film. The base substrate hillock regions are so influential in promoting the intermixing of the titanium in the sandwich layer with the carbon atoms in the diamond layer that the titanium carbide needles are even found to be touching the hillock structure of the base substrate at several points.

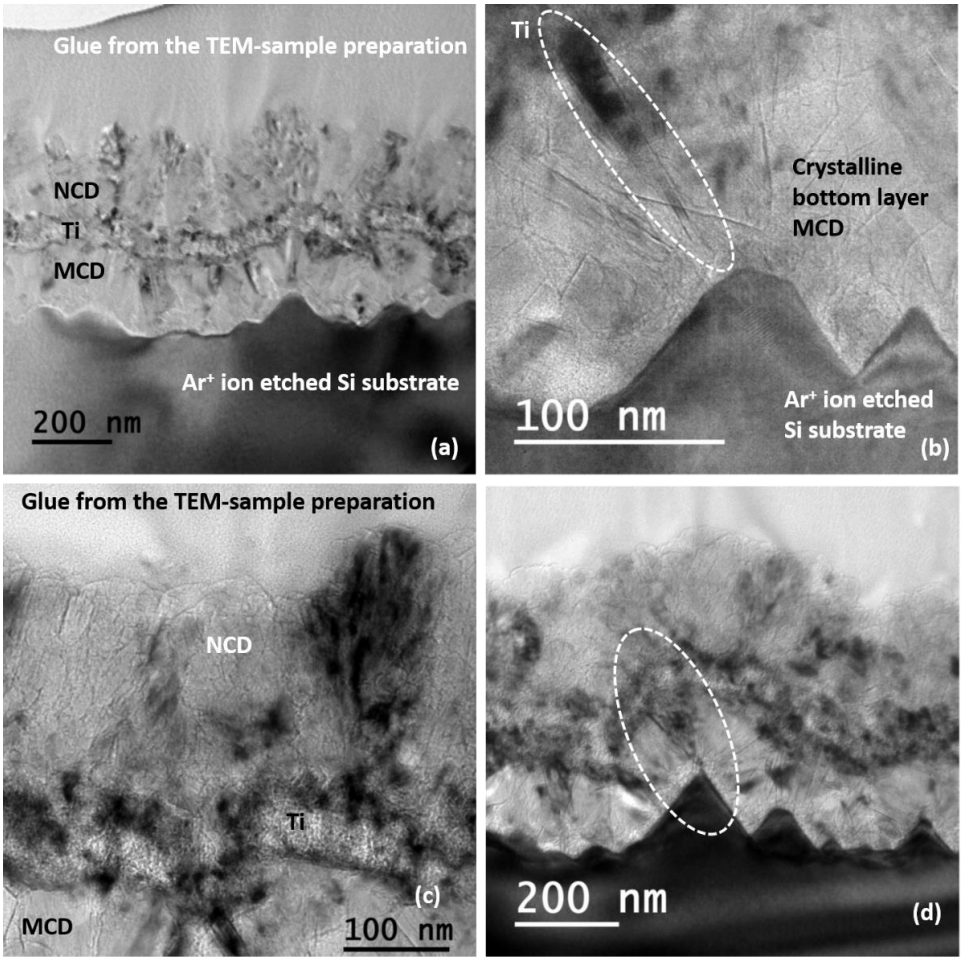

Figure 7. TEM cross-sectional images of the (**a**) MCD/Ti/NCD sandwich structure on Ar^+ plasma-etched silicon substrate, (**b**) elongated large bottom MCD crystals, (**c**) smaller grain sizes of top NCD and middle Ti layers, and (**d**) deep penetration of the Ti intermediate layer into the underlying MCD layer, even up to the bottom silicon substrate asperities.

4. Conclusions

An innovative diamond/Ti/diamond sandwich structure has been synthesised by successively following a combination of CVD and PVD routes. The base substrate was etched by Ar^+ plasma (biasing power of 150 W, and the Ar gas was flown at 100 sccm) and was found to produce deep pits and valleys (Ra = 11.7 nm, average surface roughness) onto the as-received smooth silicon surfaces (Ra = 1.7 nm). The bottom diamond layer on the base substrate, grown in an LAMWCVD reactor, (H_2, CO_2, and CH_4 gas—150 sccm volume flow, without substrate heater (400 °C), at 0.23 mTorr, 2800 W continuous wave MW input) produced a unique bi-modal film surface morphology, where MCD grains are uniformly distributed in an NCD matrix. The Ti-sputtered film was deposited (using 100 sccm Ar, power: 150 W, Ti-target, 10^{-2} Torr) onto the bottom layer of the diamond and was found to follow the underlying MCD microstructures, imprinting them into the Ti film. However, consecutive H_2 plasma treatment (for 20 min etching at 40 Torr, 3000 W microwave input power, 680 °C, 400 sccm H_2 flow inside a 2.45 GHz resonant cavity reactor) profoundly etches the Ti-MCD layer. The etching by hydrogen was so intense that the underlying diamond film became exposed, probably cracking and delaminating the sputtered Ti film (which was locally observed on the top surface, however, neither detected into the depth of the layer nor throughout the surface). However, the CVD plasma etching effectively smoothened the as-grown film surfaces and promoted the nucleation and growth of the next diamond top layer. Later, the top diamond layer was subsequently deposited by a LAMWCVD reactor (the only parameter differently used from the parameters used for the growth of the first bottom diamond layer deposition was - the addition of phosphine diluted hydrogen gas recipe at an elevated temperature of 700 °C with a heater) which promoted a nanocrystalline morphology with "cigar"-like grains with a high aspect ratio. Such deposition of the NCD layer made the hydrogen plasma-etched sputtered Ti layer surface morphology with defects invisible. The cross-sectional TEM confirms the integrity of the three-layer diamond/Ti/diamond composite film, which follows a wavy contour along the length of the sandwich structure. The diamond film microstructure can be tailor-made, either in microform or in nanocrystalline form, by changing the process gas recipe and by changing the deposition time and temperatures. Unique low-pressure and low-temperature, CVD growth does not allow for rapid film growth in the vertical z-direction. Such a well-adherent composite structure can be deposited onto many engineering surfaces for potential mechanical, thermal, electrical, and biomedical applications.

Author Contributions: A.K.M., F.L., M.G., R.R. and P.P. developed the methodology and investigated the research experiments. All the authors have reviewed and edited the work. All authors have read and agreed to the published version of the manuscript.

Funding: This work was financially supported by the Methusalem NANO network and the Research Foundation—Flanders (FWO) via project G0D4920N. A.K.M. acknowledges FWO for his Postdoctoral Fellowship with grant No. 12X2919N.

Institutional Review Board Statement: Not applicable.

Informed Consent Statement: Not applicable.

Data Availability Statement: Data are contained within the article.

Acknowledgments: All data generated or analysed during this study are included in this published article. The datasets generated during and/or analysed during the current study are available from the corresponding author on reasonable request.

Conflicts of Interest: The authors declare that they have no known competing financial interest or personal relationship that could have appeared to influence the work reported in this paper.

References

1. Rats, D.; Vandenbulcke, L.; Herbin, R.; Benoit, R.; Erre, R.; Serin, V.; Sevely, J. Characterization of diamond films deposited on titanium and its alloys. *Thin Solid Film.* **1995**, *270*, 177–183. [CrossRef]
2. Askari, S.; Chen, G.; Akhtar, F.; Lu, F. Adherent and low friction nanocrystalline diamond film grown on titanium using microwave CVD plasma. *Diam. Relat. Mater.* **2008**, *17*, 294–299. [CrossRef]
3. Zhang, X.Y.; Ma, H.L.; Zhao, Y.M.; Yao, N.; Zeng, F.G.; Zhang, B.L. Comparative studies on field emission properties of diamond and diamond /Ti films. *Adv. Mater. Res.* **2012**, *586*, 177–180. [CrossRef]
4. Veiga, C.; Davim, J.P.; Loureiro, A.J.R. Properties and applications of titanium alloys: A brief review. *Rev. Adv. Mater. Sci.* **2012**, *32*, 133–148.
5. Sundfeldt, M.; Carlsson, L.V.; Johansson, C.B.; Thomsen, P.; Gretzer, C. Aseptic loosening, not only a question of wear: A review of different theories. *Acta Orthop.* **2006**, *77*, 177–197. [CrossRef]
6. Rifai, A.; Tran, N.; Lau, D.W.; Elbourne, A.; Zhan, H.; Stacey, A.D.; Mayes, E.L.H.; Sarker, A.; Ivanova, E.P.; Crawford, R.J.; et al. Polycrystalline Diamond Coating of Additively Manufactured Titanium for Biomedical Applications. *ACS Appl. Mater. Interfaces* **2018**, *10*, 8474–8484. [CrossRef] [PubMed]
7. Rifai, A.; Tran, N.; Reineck, P.; Elbourne, A.; Mayes, E.L.H.; Sarker, A.; Dekiwadia, C.; Ivanova, E.P.; Crawford, R.J.; Ohshima, T.; et al. Engineering the Interface: Nanodiamond Coating on 3D-Printed Titanium Promotes Mammalian Cell Growth and Inhibits Staphylococcus aureus Colonization. *ACS Appl. Mater. Interfaces* **2019**, *11*, 24588–24597. [CrossRef] [PubMed]
8. Fox, K.; Mani, N.; Rifai, A.; Reineck, P.; Jones, A.; Tran, P.A.; Ramezannejad, A.; Brandt, M.; Gibson, B.C.; Greentree, A.D.; et al. 3D-Printed Diamond–Titanium Composite: A Hybrid Material for Implant Engineering. *ACS Appl. Bio Mater.* **2020**, *3*, 29–36. [CrossRef]
9. Van Noort, R. Titanium: The implant material of today. *J. Mater. Sci.* **1987**, *22*, 3801–3811. [CrossRef]
10. Zhao, L.; Chu, P.K.; Zhang, Y.; Wu, Z. Antibacterial coatings on titanium implants. *J. Biomed. Mater. Res. Part B* **2009**, *91*, 470–480. [CrossRef] [PubMed]
11. Skoog, S.A.; Kumar, G.; Zheng, J.; Sumant, A.V.; Goering, P.L.; Narayan, R.J. Biological evaluation of ultrananocrystalline and nanocrystalline diamond coatings. *J. Mater. Sci. Mater. Med.* **2016**, *27*, 187. [CrossRef]
12. Jana, A.; Dandapat, N.; Sengupta, S.; Balla, V.K.; Saha, R.; Mallik, A.K. Human osteoblast like MG63 cell and mouse fibroblast NIH3T3 cell viability study on the nucleation side of CVD grown polycrystalline diamond coatings. *Trends Biomater. Artif. Organs* **2015**, *29*, 211–216.
13. Ahnood, A.; Meffin, H.; Garrett, D.J.; Fox, K.; Ganesan, K.; Stacey, A.; Apollo, N.V.; Wong, Y.T.; Lichter, S.G.; Kentler, W.; et al. Diamond Devices for High Acuity Prosthetic Vision. *Adv. Biosyst.* **2017**, *1*, 1600003. [CrossRef] [PubMed]
14. Yan, B.; Loh, N.L.; Fu, Y.; Sun, C.Q.; Hing, P. Surface and interface characterization of diamond coatings deposited on pure titanium. *Surf. Coat. Technol.* **1999**, *115*, 256–265. [CrossRef]
15. Kulesza, S.; Patyk, J.; Daenen, M.; Williams, O.; Van de Putte, W.; Fransaer, J.; Haenen, K.; Nesládek, M. Structural investigations of protective polycrystalline diamond coatings on titanium substrates. *Surf. Coat. Technol.* **2006**, *201*, 203–207. [CrossRef]
16. Li, Y.; Yang, L.; Tang, Y.; Zhang, C.; Zhang, L.; Onyeka, I.; Yang, Q.; Feng, R.; Hirose, A. Adherent nanocrystalline diamond coatings deposited on Ti substrate at moderate temperatures. *Surf. Coat. Technol.* **2011**, *206*, 1971–1976. [CrossRef]
17. Li, Y.; Zhang, C.; Ma, H.; Yang, L.; Zhang, L.; Tang, Y.; Li, X.; He, L.; Feng, R.; Yang, Q.; et al. CVD nanocrystalline diamond coatings on Ti alloy: A synchrotron-assisted interfacial investigation. *Mater. Chem. Phys.* **2012**, *134*, 145–152. [CrossRef]
18. Li, X.; Li, Y.; He, L.; Yang, Q.; Hirose, A. Fine structures study of the diamond/titanium interface by transmission electron microscopy. *Mater. Chem. Phys.* **2014**, *143*, 647–652. [CrossRef]
19. Zhang, C.; Niakan, H.; Yang, L.; Li, Y.; Hu, Y.; Yang, Q. Study of diamond nucleation and growth on Ti6Al4V with tungsten interlayer. *Surf. Coat. Technol.* **2013**, *237*, 248–254. [CrossRef]
20. Fu, Y.; Yan, B.; Loh, N.L. Effects of pre-treatments and interlayers on the nucleation and growth of diamond coatings on titanium substrates. *Surf. Coat. Technol.* **2000**, *130*, 173–185. [CrossRef]
21. Yang, B.; Li, H.; Yu, B.; Huang, N.; Liu, L.; Jiang, X. Deposition of highly adhesive nanocrystalline diamond films on Ti substrates via diamond/SiC composite interlayers. *Diam. Relat. Mater.* **2020**, *108*, 107928. [CrossRef]
22. Wang, T.; Zhuang, H.; Jiang, X. One step deposition of highly adhesive diamond films on cemented carbide substrates via diamond/beta-SiC composite interlayers. *Appl. Surf. Sci.* **2015**, *359*, 790–796. [CrossRef]
23. Lessiak, M.; Haubner, R. Diamond coatings on hardmetal substrates with CVD coatings as intermediate layers. *Surf. Coat. Technol.* **2013**, *230*, 119–123. [CrossRef]
24. Fu, Y.; Loh, N.L.; Yan, B.; Sun, C.Q.; Hing, P. Control of microstructure coarsening of a Ti substrate during diamond film deposition using Ar/H-2/CH4 gas mixture. *Thin Solid Film.* **2000**, *359*, 215. [CrossRef]
25. Tamburri, E.; Carcione, R.; Vitale, F.; Valguarnera, A.; Macis, S.; Lucci, M.; Terranova, M.L. Exploiting the Properties of Ti-Doped CVD-Grown Diamonds for the Assembling of Electrodes. *Adv. Mater. Interfaces* **2017**, *4*, 1700222. [CrossRef]
26. Zhang, Y.; Wang, X.T.; Jiang, S.B.; Wu, J.H. Thermo-physical properties of Ti-coated diamond/Al composites prepared by pressure infiltration. *Mater. Sci. Forum* **2010**, *654–656*, 2572–2575. [CrossRef]
27. Roy, S.; Das, M.; Mallik, A.K.; Balla, V.K. Laser melting of titanium-diamond composites: Microstructure and mechanical behavior study. *Mater. Lett.* **2016**, *178*, 284–287. [CrossRef]

28. Liu, J.L.; Li, C.M.; Chen, L.X.; Zhang, Y.Y.; Hei, L.F.; Lv, F.X. Preparation and characterization of diamond-TiC-Ti-Ag/Cu gradient metallization system. *Mater. Sci. Forum* **2011**, *687*, 722–728. [CrossRef]
29. Liu, D.; Zhou, Y.; Song, X.; Huo, W.; Feng, J. Interfacial microstructure and performance of nano-diamond film/Ti-6Al-4V joint brazed with AgCuTi alloy. *Diam. Relat. Mater.* **2016**, *68*, 42–50. [CrossRef]
30. Chen, Y.; Su, H.H.; Fu, Y.C.; Guo, Z. Investigation of inferface microstructure of diamond and Ti coated diamond brazed with Cu-Sn-Ti alloy. *Key Eng. Mater.* **2011**, *487*, 199–203. [CrossRef]
31. Jin, Y.; Wu, W.; Li, L.; Chen, J.; Zhang, J.; Zuo, Y.; Fu, J. Effect of sputtering power on surface topography of dc magnetron sputtered Ti thin films observed by AFM. *Appl. Surf. Sci.* **2009**, *255*, 4673–4679. [CrossRef]
32. Wadge, M.D.; Turgut, B.; Murray, J.W.; Stuart, B.W.; Felfel, R.M.; Ahmed, I.; Grant, D.M. Developing highly nanoporous titanate structures via wet chemical conversion of DC magnetron sputtered titanium thin films. *J. Colloid Interface Sci.* **2020**, *566*, 271–283. [CrossRef] [PubMed]
33. Zhang, L.; Shi, L.; He, Z.; Zhang, B.; Lu, Y.; Liu, A.; Wang, B. Deposition of dense and smooth Ti films using ECR plasma-assisted magnetron sputtering. *Surf. Coat. Technol.* **2009**, *203*, 3356–3360. [CrossRef]
34. Chawla, V.; Jayaganthan, R.; Chawla, A.; Chandra, R. Microstructural characterizations of magnetron sputtered Ti films on glass substrate. *J. Mater. Process. Technol.* **2009**, *209*, 3444–3451. [CrossRef]
35. Fontana, L.C.; Muzart, J.L.R. Characteristics of triode magnetron sputtering: The morphology of deposited titanium films. *Surf. Coat. Technol.* **1998**, *107*, 24–30. [CrossRef]
36. Tankut, A.; Miller, K.E.; Ohuchi, F.S. PVD Ti-films for plasma-facing first walls, Part I: Characterization of surface chemistry during H_2 and O_2 exposure. *J. Nucl. Mater.* **2013**, *433*, 404–411. [CrossRef]
37. Sha, X.; Yue, W.; Zhang, H.; Qin, W.; She, D.; Wang, C. Enhanced oxidation and graphitization resistance of polycrystalline diamond sintered with Ti-coated diamond powders. *J. Mater. Sci. Technol.* **2020**, *43*, 64–73. [CrossRef]
38. Zhang, S.; Fu, Y.; Du, H.; Zeng, X.; Liu, Y. Magnetron sputtering of nanocomposite (Ti,Cr)CN/DLC coatings. *Surf. Coat. Technol.* **2003**, *162*, 42–48. [CrossRef]
39. Liu, X.; Lu, P.; Wang, H.; Ren, Y.; Tan, X.; Sun, S.; Jia, H. Morphology and structure of Ti-doped diamond films prepared by microwave plasma chemical vapor deposition. *Appl. Surf. Sci.* **2018**, *442*, 529–536. [CrossRef]
40. Qiang, L.; Zhang, B.; Zhou, Y.; Zhang, J. Improving the internal stress and wear resistance of DLC film by low content Ti Doping. *Solid State Sci.* **2013**, *20*, 17–22. [CrossRef]
41. Drory, M.D.; Hutchinson, J.W. Diamond coating of Ti Alloys. *Science* **1994**, *263*, 1753. [CrossRef] [PubMed]
42. Buccioni, E.; Braca, E.; Kenny, J.; Terranova, M. Processing–structure–adhesion relationship in CVD diamond films on titanium substrates. *Diam. Relat. Mater.* **1999**, *8*, 17–24. [CrossRef]
43. Janssen, W.; Turner, S.; Sakr, G.; Jomard, F.; Barjon, J.; Degutis, G.; Lu, Y.-G.; D'Haen, J.; Hardy, A.; Van Bael, M.; et al. Substitutional phosphorus incorporation in nanocrystalline CVD diamond thin films. *Phys. Status Solidi* **2014**, *8*, 705–709. [CrossRef]
44. Harniman, R.L.; Fox, O.J.; Janssen, W.; Drijkoningen, S.; Haenen, K.; May, P.W. Direct observation of electron emission from grain boundaries in CVD diamond by PeakForce-controlled tunnelling atomic force microscopy. *Carbon* **2015**, *94*, 386–395. [CrossRef]
45. Pobedinskas, P.; Degutis, G.; Dexters, W.; Janssen, W.; Janssens, S.D.; Conings, B.; Ruttens, B.; D'Haen, J.; Boyen, H.-G.; Hardy, A.; et al. Surface plasma pretreatment for enhanced diamond nucleation on AlN. *Appl. Phys. Lett.* **2013**, *102*, 201609. [CrossRef]
46. Pobedinskas, P.; Degutis, G.; Dexters, W.; D'haen, J.; Van Bael, M.; Haenen, K. Nanodiamond seeding on plasma-treated tantalum thin films and the role of surface contamination. *Appl. Surf. Sci.* **2021**, *538*, 148016. [CrossRef]
47. Drijkoningen, S.; Pobedinskas, P.; Korneychuk, S.; Momot, A.; Balasubramaniam, Y.; Van Bael, M.K.; Turner, S.; Verbeeck, J.; Nesládek, M.; Haenen, K. On the origin of diamond plates deposited at low temperature. *Cryst. Growth Des.* **2017**, *17*, 4306. [CrossRef]
48. Lloret, F.; Sankaran, K.J.; Millan-Barba, J.; Desta, D.; Rouzbahani, R.; Pobedinskas, P.; Gutierrez, M.; Boyen, H.-G.; Haenen, K. Improved Field Electron Emission Properties of Phosphorus and Nitrogen Co-Doped Nanocrystalline Diamond Films. *Nanomaterials* **2020**, *10*, 1024. [CrossRef]
49. Rabinovich, Y.I.; Adler, J.J.; Ata, A.; Singh, R.K.; Moudgil, B.M. Adhesion between Nanoscale Rough Surfaces: I. Role of Asperity Geometry. *J. Colloid Interface Sci.* **2000**, *232*, 10–16. [CrossRef] [PubMed]
50. Ferrari, A.C.; Robertson, J. Raman spectroscopy of amorphous, nanostructured, diamond–like carbon, and nanodiamond. *Phil. Trans. R. Soc. A* **2004**, *362*, 2477–2512. [CrossRef]
51. Pal, K.S.; Mallik, A.K.; Dandapat, N.; Ray, N.R.; Datta, S.; Bysakh, S.; Guha, B.K. Microscopic properties of MPCVD diamond coatings studied by micro-Raman and micro-photoluminescence spectroscopy. *Bull. Mater. Sci.* **2015**, *38*, 537–549. [CrossRef]
52. Degutis, G.; Pobedinskas, P.; Turner, S.; Lu, Y.-G.; Al Riyami, S.; Ruttens, B.; Yoshitake, T.; D'Haen, J.; Haenen, K.; Verbeeck, J.; et al. CVD diamond growth from nanodiamond seeds buried under a thin chromium layer. *Diam. Relat. Mater.* **2016**, *64*, 163–168. [CrossRef]
53. Daenen, M.; Zhang, L.; Erni, R.; Williams, O.A.; Hardy, A.; Van Bael, M.K.; Wagner, P.; Haenen, K.; Nesládek, M.; Van Tendeloo, G. Diamond nucleation by carbon transport from buried nanodiamond TiO_2 sol-gel composites. *Adv. Mater.* **2009**, *21*, 670–673. [CrossRef]

54. Lu, Y.-G.; Verbeeck, J.; Turner, S.; Hardy, A.; Janssens, S.D.; De Dobbelaere, C.; Wagner, P.; Van Bael, M.K.; Haenen, K.; Van Tendeloo, G. Analytical TEM study of CVD diamond growth on TiO_2 sol-gel layers. *Diam. Relat. Mater.* **2012**, *23*, 93–99. [CrossRef]
55. Sankaran, K.J.; Yeh, C.-J.; Hsieh, P.-Y.; Pobedinskas, P.; Kunuku, S.; Leou, K.-C.; Tai, N.-H.; Lin, I.-N.; Haenen, K. Origin of Conductive Nanocrystalline Diamond Nanoneedles for Optoelectronic Applications. *ACS Appl. Mater. Interfaces* **2019**, *11*, 25388–25398. [CrossRef] [PubMed]